Updated estimate of aerosol direct radiative forcing from satellite observations and comparison against the Hadley Centre climate model

Article

Published Version

Updated estimate of aerosol direct radiative forcing from satellite observations and comparison against the Hadley Centre climate model

Nicolas Bellouin,[1] Andy Jones,[1] Jim Haywood,[1] and Sundar A. Christopher[2]

[1] The fourth assessment report of the Intergovernmental Panel on Climate Change (IPCC) includes a comparison of observation-based and modeling-based estimates of the aerosol direct radiative forcing. In this comparison, satellite-based studies suggest a more negative aerosol direct radiative forcing than modeling studies. A previous satellite-based study, part of the IPCC comparison, uses aerosol optical depths and accumulation-mode fractions retrieved by the Moderate Resolution Imaging Spectroradiometer (MODIS) at collection 4. The latest version of MODIS products, named collection 5, improves aerosol retrievals. Using these products, the direct forcing in the shortwave spectrum defined with respect to present-day natural aerosols is now estimated at -1.30 and -0.65 Wm^{-2} on a global clear-sky and all-sky average, respectively, for 2002. These values are still significantly more negative than the numbers reported by modeling studies. By accounting for differences between present-day natural and preindustrial aerosol concentrations, sampling biases, and investigating the impact of differences in the zonal distribution of anthropogenic aerosols, good agreement is reached between the direct forcing derived from MODIS and the Hadley Centre climate model HadGEM2-A over clear-sky oceans. Results also suggest that satellite estimates of anthropogenic aerosol optical depth over land should be coupled with a robust validation strategy in order to refine the observation-based estimate of aerosol direct radiative forcing. In addition, the complex problem of deriving the aerosol direct radiative forcing when aerosols are located above cloud still needs to be addressed.

1. Introduction

[2] Radiative forcing has been used as an indicator of the potential climate response because global modeling studies suggest that forcing is approximately linearly related to global mean equilibrium temperature change. For a given perturbing agent, the radiative forcing of the surface-troposphere system is the change in net irradiance at the tropopause after allowing for stratospheric temperatures to readjust to radiative equilibrium but with surface and tropospheric temperatures and other state variables held fixed at the unperturbed values [*Forster et al.*, 2007]. Anthropogenic aerosols exert a direct radiative forcing (DRF) by scattering and absorbing incoming solar and outgoing long-wave radiation. Hereafter, DRF estimates considered here are in the shortwave spectrum only.

[3] Modeling studies can diagnose the DRF by differencing irradiances obtained by running a general circulation model (GCM) twice, first including present-day aerosols,

then preindustrial aerosols. In each run, the radiative transfer code is called twice. The first call includes scattering and absorption of radiation by aerosols; the second does not and is used for advancing the model into its next timestep. By doing so, surface and tropospheric temperatures are held fixed for the DRF calculation and the model evolution is unaffected by aerosols. The DRF of tropospheric aerosols is most often determined at the top of the atmosphere rather than the tropopause and stratospheric adjustment is ignored. The relaxation of both of these assumptions is thought to have little influence on the diagnosed DRF for tropospheric aerosols [*Forster et al.*, 2007]. Reporting the results of the AeroCom project, an intercomparison of numerical modeling of aerosols, *Schulz et al.* [2006] estimate the DRF with respect to pre-industrial conditions at -0.2 ± 0.2 Wm^{-2}. Including the effect of anthropogenic nitrate and mineral dust aerosols, which are not explicitly modeled by many AeroCom-participating models, suggests a DRF by anthropogenic aerosols of -0.4 ± 0.4 Wm^{-2} [*Forster et al.*, 2007].

[4] Well-validated retrievals of aerosol properties from satellites have only been developed over the last decade [e.g., *Kaufman et al.*, 2002], which leads to a problem when attempting to derive the DRF: the preindustrial aerosol concentrations cannot be inferred from the satellite measurements alone. Alternative approaches have therefore been

---

[1]Met Office Hadley Centre, Exeter, UK.
[2]Department of Atmospheric Sciences, University of Alabama, Huntsville, Alabama, USA.

Table 1. Aerosol Direct Radiative Forcing (Wm^{-2}) in the Shortwave Spectrum Estimated by Observation-Based Studies and Reviews of Modeling Studies

Reference	Clear-Sky Ocean	Clear-Sky Global	All-Sky Global
Kaufman et al. [2005]	-1.4 ± 0.4		
Christopher et al. [2006]	-1.4 ± 0.9		
Yu et al. [2004]	-1.3	-1.4	
Chung et al. [2005]		-1.1	-0.6 to -0.1
Bellouin et al. [2005]	-0.8 ± 0.1	-1.9 ± 0.3	-0.8 ± 0.1
Schulz et al. [2006]	-0.6 ± 0.2	-0.7 ± 0.3	-0.2 ± 0.2
Forster et al. [2007]			-0.4 ± 0.4

used, for example by considering present-day natural aerosols as an approximation of preindustrial conditions. Aerosol retrievals are not performed in cloudy skies, and the uncertainty in the retrieved values is less over dark surfaces such as ocean and vegetation. For these reasons, satellite-based studies limit themselves to clear-sky (i.e., cloud-free) conditions, and make various assumptions when scaling the clear-sky forcing to an all-sky (clear plus cloudy) value. Table 1 shows satellite-based estimates of the aerosol DRF by several studies using different methods. Limiting themselves to clear-sky oceans where satellite retrievals of aerosol properties are most accurate, *Kaufman et al.* [2005] and *Christopher et al.* [2006] both derive a DRF of -1.4 Wm^{-2}. The former used satellite-retrievals combined with aerosol radiative forcing efficiencies while the latter used a combination of aerosol retrievals and broadband-flux measurements from satellite instruments. *Yu et al.* [2004] and *Chung et al.* [2005] used a combination of GCM simulations and satellite observations. *Bellouin et al.* [2005], the study that arguably relies most on satellite and ground-based observations and the least on GCMs, while still including land areas, gives the strongest DRF at -0.8 Wm^{-2} on a global all-sky average; this study is described in the next section. Also shown in Table 1 are corresponding modeling estimates from *Schulz et al.* [2006]

and *Forster et al.* [2007]. Note that only *Chung et al.* [2005] and *Bellouin et al.* [2005] estimate the DRF for all-sky global conditions and, as documented by *Forster et al.* [2007], these studies suggest a stronger DRF than those derived from models.

[5] In this study, we refine the results of *Bellouin et al.* [2005], hereafter abbreviated BBHR, by using updated satellite retrievals and compare them against results from the Hadley Centre climate model HadGEM2-A to try to reconcile the results from both approaches.

2. Satellite-Based Estimates From MODIS

2.1. Anthropogenic Aerosol Optical Depth

[6] Since preindustrial observations of aerosols are not available, BBHR estimates the radiative forcing exerted by present-day anthropogenic aerosols with respect to present-day natural aerosols. The aerosol optical depth (AOD) of anthropogenic aerosols is defined as the difference between the present-day total AOD and its natural component. The Moderate Resolution Imaging Spectroradiometer (MODIS) retrieves the total AOD (τ_{total}) over cloud-free oceans and land surfaces (except bright surfaces such as deserts and snow-covered areas) and the accumulation-mode fraction (AMF) over oceans only [*Remer et al.*, 2005]. The AMF is the fraction of the total AOD due to aerosols smaller than 1 μm in diameter. BBHR used aircraft and ground-based Sun-photometer measurements to demonstrate that industrial and biomass-burning aerosols (assumed anthropogenic) are associated with larger AMFs than mineral dust and sea-salt aerosols (assumed natural).

[7] Figure 1 shows a schematic flow chart of the logic used in the algorithm over oceans. The total AOD is partitioned into three components corresponding to anthropogenic, mineral dust and sea-salt aerosols using a combination of AMF and the Total Ozone Mapping Spectroradiometer (TOMS) [*Herman et al.*, 1997] absorbing aerosol index (AI). These component AODs are denoted τ_{anthr}, τ_{dust} and τ_{salt}, respectively. The sea-salt AOD is computed from the
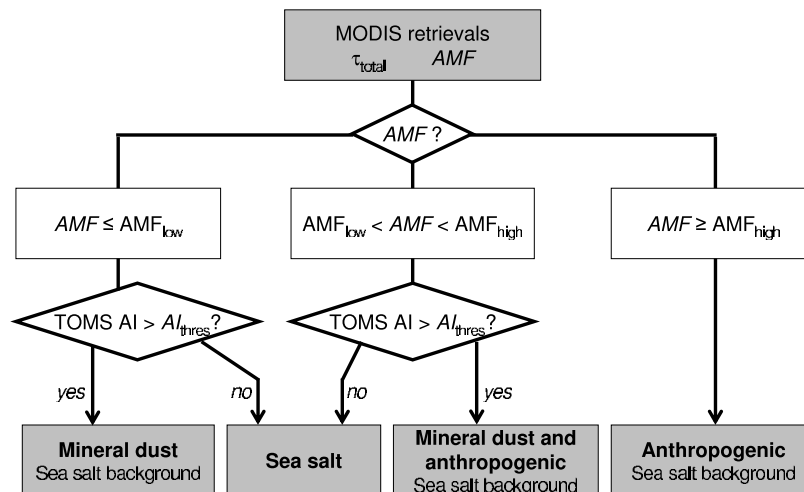
Figure 1. Flow diagram of the algorithm used to identify sea-salt, mineral dust, and anthropogenic aerosols from MODIS measurements of the total aerosol optical depth (τ_{total}) and accumulation-mode fraction (AMF) over the ocean. AMF$_{low}$ and AMF$_{high}$ are thresholds on the accumulation-mode fraction. AI_{thres} is a threshold on the TOMS absorbing aerosol index (AI).

near-surface wind speed (w in ms^{-1}) following *Smirnov et al.* [2003]:

$$\tau_{salt} = 0.006\ w\ +\ 0.060. \tag{1}$$

w is measured by the Special Sensor Microwave Imager (SSM/I) [*Wentz*, 1997]. As equation (1) is an approximation of a complex relationship between sea-salt production and wind speed, it may lead to sea-salt AODs that are larger than the retrieved total AOD. In this case, sea-salt becomes the only identified aerosol at an AOD equal to the total AOD. For AMFs larger than AMF$_{high}$ = 0.83, the aerosol is assumed to be anthropogenic and τ_{anthr} is the total AOD corrected for the sea-salt background AOD:

$$\tau_{anthr} = \tau_{total} - \tau_{salt} \tag{2}$$

Natural aerosols are identified for AMFs smaller than AMF$_{low}$ = 0.35. The fact that mineral dust absorbs in the UV while sea-salt does not is used to discriminate further between those two species. UV absorption is detected by TOMS: where the monthly-averaged TOMS AI is larger than a detection threshold, set to 1, the sea-salt AOD is computed from equation (1) and the mineral dust AOD is the residual:

$$\tau_{dust} = \tau_{total} - \tau_{salt} \tag{3}$$

The intermediate category where AMFs lie between the two thresholds is more difficult to characterize, since any mixture of anthropogenic aerosols with either or both mineral dust and sea-salt can exhibit such AMFs. TOMS detection of UV-absorbing aerosols (mineral dust and/or biomass-burning) is again used. Where the TOMS AI is larger than the detection threshold, mineral dust and anthropogenic aerosols are given the coarse- and accumulation-mode optical depth, respectively, after correcting for the sea-salt contribution (equation (1)):

$$\tau_{dust} = (1 - AMF)\ (\tau_{total} - \tau_{salt}) \tag{4}$$

$$\tau_{anthr} = AMF(\tau_{total} - \tau_{salt}) \tag{5}$$

Where the TOMS AI is smaller than the detection threshold, the total AOD is attributed to sea-salt. Consequently, pollution events composed of aerosols that do not absorb in the UV (e.g., sulphate) and are not thick enough to significantly affect the retrieved AMF will be identified as sea-salt.

[8] Over land, where the AMF is not reliably retrieved, regional anthropogenic fractions are obtained from five general circulation and chemistry transport models that participated in the AeroCom project. Models are LMDzt [*Reddy et al.*, 2005], SPRINTARS [*Takemura et al.*, 2005], ECHAM5-HAM [*Stier et al.*, 2005], MATCH [*Collins et al.*, 2002], and the general circulation model of the University of Oslo [*Kirkevag and Iversen*, 2002]. Regional values of the anthropogenic fraction are given in BBHR. The natural aerosol type is not formally identified. Anthropogenic fractions over land are the only quantities not directly derived from observations.

2.2. Direct Radiative Forcing

[9] Once the anthropogenic AOD has been identified, it is converted into a DRF through radiative transfer calculations. This conversion requires the knowledge of the aerosol optical properties, the surface albedo, and the aerosol vertical profile. Aerosol optical properties are derived from size distributions and single-scattering albedos retrieved from ground-based Sun-photometer measurements at specific sites worldwide (BBHR) [*Dubovik et al.*, 2002]; such sites are assumed to be representative of a wider area. Over land, the unidentified natural aerosol is assumed to have the same optical properties as the anthropogenic one, which is reasonable for most locations but is not true where mineral dust contributes largely to the natural AOD. However, those locations include mostly deserts where MODIS retrievals are not attempted. The surface albedo is computed over ocean [*Cox and Munk*, 1954] and derived from MODIS observations over land [*Schaaf et al.*, 2002]. Finally, the aerosol vertical profile is assumed since it is not yet routinely measured on a global scale. The assumption is that natural aerosols are located in the first kilometer of the atmosphere, below a layer of anthropogenic aerosols. Where there are only anthropogenic aerosols in the atmosphere, the impact of this assumed vertical profile on the shortwave radiative fluxes at the top of the atmosphere is small: the change in Rayleigh scattering above the aerosol layer is a second-order effect. However, where natural aerosols are also present, their own direct effect will modify the radiative fluxes experienced by anthropogenic aerosols, and therefore their DRF. Assuming that natural aerosols underlie the anthropogenic layer effectively increases the reflectance of the underlying atmosphere, and makes the DRF less negative than when other vertical profiles are used.
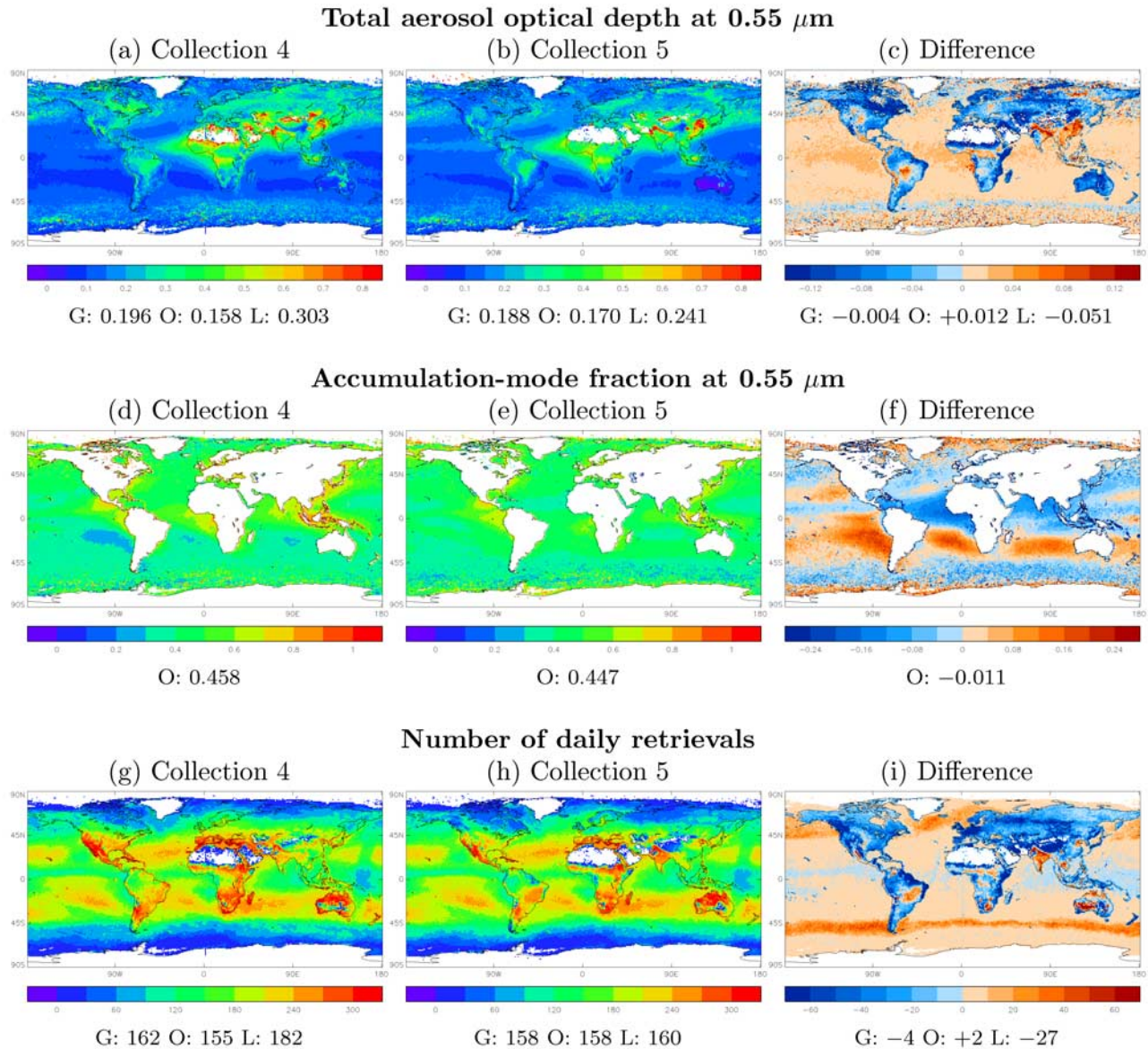
[10] Radiative transfer calculations are performed for clear-sky conditions. However, in order to provide all-sky estimates, the clear-sky values are scaled to all-sky by multiplying by the complement of the fractional cloud cover. Doing so assumes that the DRF of aerosols in cloudy skies is zero. This assumption is discussed later.

2.3. Changes to MODIS Aerosol Products

[11] BBHR used MODIS/Terra daily products (MOD08_D3) given on a 1° by 1° grid from collection 4 for the year 2002. Collection 5 data are now available. Changes include a better correction of the surface contribution to the measured signal, assumed aerosol models now based on regional Sun-photometer measurements, and improved snow and cloud masking [*Levy et al.*, 2007]. The biases reported by collection 4 validation studies [*Remer et al.*, 2005] are much reduced in collection 5. Annual distributions of the total AOD and the AMF for the year 2002 from the two collections and their difference are shown in Figure 2. Note that the distributions of the differences have missing data where at least one collection does not have a retrieval. Also shown are the number of daily retrievals included in the annual average. A detailed explanation of why these changes occur is given by *Levy et al.* [2007]. We focus here on the impact of those changes on the estimated anthropogenic AOD and DRF using the above algorithm.

[12] For 2002, the switch to collection 5 has three main consequences. First, the AOD over land decreases from 0.30 to 0.24 on an annual average. Over ocean, the change

Total aerosol optical depth at 0.55 μm

(a) Collection 4   (b) Collection 5   (c) Difference

G: 0.196 O: 0.158 L: 0.303   G: 0.188 O: 0.170 L: 0.241   G: −0.004 O: +0.012 L: −0.051

Accumulation-mode fraction at 0.55 μm

(d) Collection 4   (e) Collection 5   (f) Difference

O: 0.458   O: 0.447   O: −0.011

Number of daily retrievals

(g) Collection 4   (h) Collection 5   (i) Difference

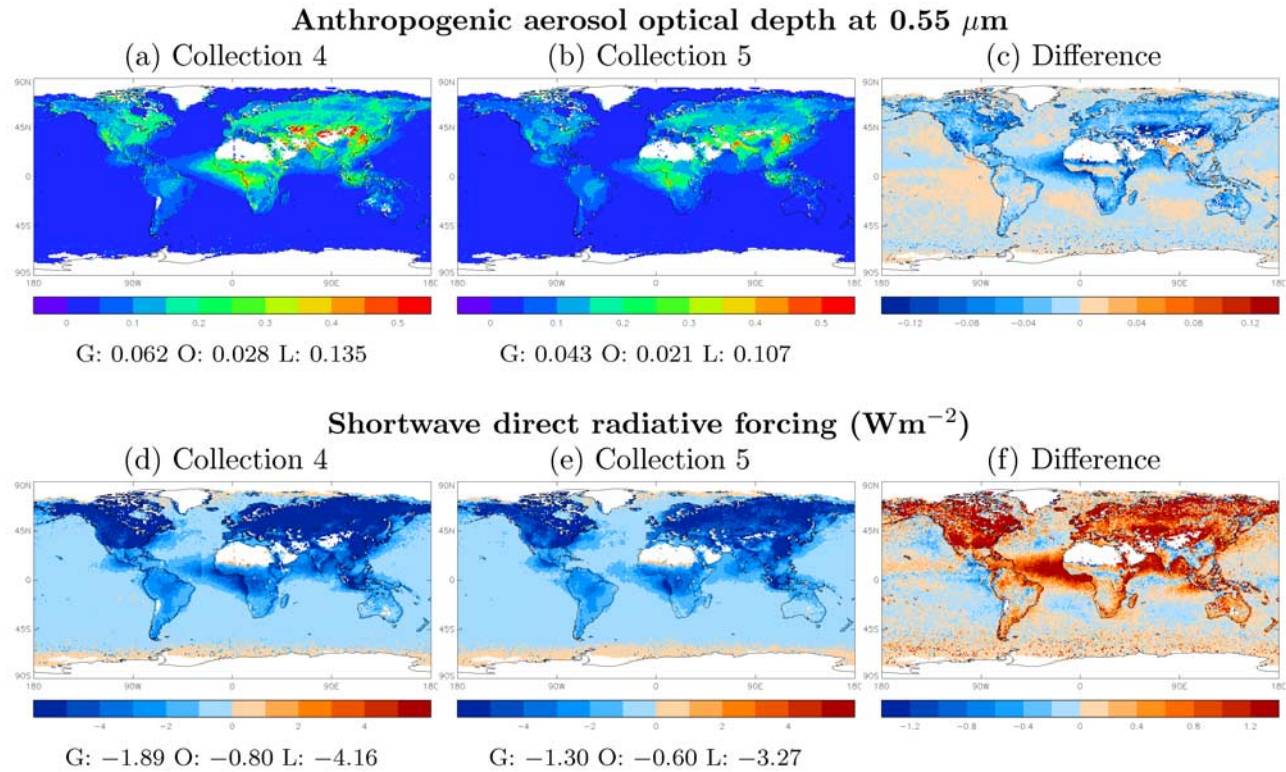G: 162 O: 155 L: 182   G: 158 O: 158 L: 160   G: −4 O: +2 L: −27

Figure 2. Distributions of aerosol retrievals from MODIS collections 4 (left) and 5 (middle) and their difference (right, positive values where collection 5 contains larger values than collection 4). All distributions are annual means for the year 2002. Averages are given on a global (G), ocean-only (O), and land-only (L) basis.

in AOD is less significant, from 0.16 to 0.17. Second, although the annual-averaged AMF over ocean does not change significantly, there are significant local changes. As seen in Figure 2, the AMFs have decreased in the mineral dust regions where the threshold on the TOMS AI will trigger the algorithm into identifying non-sea-salt species. The erroneous identification of mineral dust was estimated by BBHR to lead to errors in the global DRF of up to 5%; these errors are rectified when using collection 5 data. Third, because the conditions for a successful retrieval over land are more stringent, the number of daily retrievals in collection 5 has gone down by 27 days per year on average, compared with collection 4. The relative contributions of ocean and land surfaces to the global mean have therefore changed. Whereas daily retrievals are available for half of

the year over oceans and tropical land masses, northern hemisphere land surfaces are underrepresented.

2.4. Updated Estimates

[13] Anthropogenic AODs and the corresponding DRFs are shown on Figure 3 for collection 4 and 5 and the difference between the two. Over ocean, using collection 4 leads to an anthropogenic AOD of 0.028 and a clear-sky DRF of −0.80 Wm^{-2}; using collection 5, those decrease to 0.021 and −0.60 Wm^{-2}, respectively. The decrease mostly happens in areas where mineral dust is present and is a consequence of the change in AMF of mineral dust plumes. On a global average, using collection 4 leads to an anthropogenic AOD of 0.062 and a DRF of −1.89 Wm^{-2} in clear-sky and −0.77 for all-sky; the values obtained from collection 5 are 0.043, −1.30 and −0.65 Wm^{-2}, respectively. The decrease

Anthropogenic aerosol optical depth at 0.55 μm

G: 0.062 O: 0.028 L: 0.135   G: 0.043 O: 0.021 L: 0.107

Shortwave direct radiative forcing (Wm^{-2})

G: −1.89 O: −0.80 L: −4.16   G: −1.30 O: −0.60 L: −3.27

Figure 3. Distributions of the anthropogenic aerosol optical depth and clear-sky shortwave direct radiative forcing as derived from MODIS retrievals for collection 4 (left) and 5 (middle), and their difference (right, coll. 5 minus coll. 4). All distributions are annual means for the year 2002. Averages are given on a global (G), ocean-only (O), and land-only (L) basis.

in total AOD over land and the change in the number of available daily retrievals are the cause of these changes: 75% of processed scenes are over oceans in collection 5 and this number exhibits large monthly variations. Owing to limitations in observing northern hemisphere continents in winter, northern hemisphere winter months are associated with the largest ocean contribution (around 80% of processed points), whereas that value is around the expected 70% for summer months.

3. Aerosols and Direct Forcing in HadGEM2-A

[14] As noted in the introduction, there are some differences in the formulation of the DRF between the measurement-based estimates and those from models. To investigate the potential impact of these we use the HadGEM2-A model which is the atmospheric component of the Hadley Centre Global Environmental Model version 2. Compared with the previous version of that model, HadGAM1, described by *Martin et al.* [2006], aerosols have been improved and new species added [*Bellouin et al.*, 2007]. HadGEM2-A includes six aerosol species. Four of them were present in HadGAM1: sulphate and biomass-burning, which have been improved for HadGEM2-A, and black carbon and sea-salt. Two new species have been introduced: mineral dust and a climatology of secondary organic aerosol from biogenic terpene emissions. When compared with ground-based Sun-photometer measurements, the model underestimates the AOD over Europe and North America in winter

and northwestern Africa during mineral dust and biomass-burning events. However, simulations are good during summer and throughout the year in Asia, southern Africa, and South America [*Bellouin et al.*, 2007].

[15] The total AOD at 0.55 μm is 0.110 in present-day conditions and 0.080 for 1860 emissions, an increase of 0.030. The change in AOD between present-day and 1860 simulations is shown in Figure 4a. The industrial and biomass-burning regions of the world are clearly visible on this distribution. Interestingly, some areas of eastern Russia and northern Canada exhibit a decrease in AOD since 1860. This is due to the biomass-burning emission data set that assumes that fire suppression policies have become more effective since preindustrial times [*Dentener et al.*, 2006]. The change in optical depth since 1860 translates into a shortwave direct forcing of −0.16 Wm^{-2} in all-sky and −0.63 Wm^{-2} in clear-sky, on a global average. Over clear-sky oceans, it is −0.51 Wm^{-2}. These values are similar to those obtained by the AeroCom models, given in Table 1, justifying the use of this model as being reasonably representative of those used in the IPCC assessment report [*Forster et al.*, 2007]. Of course, the precise geographic distribution of the forcing will differ between models as discussed by *Schulz et al.* [2006].

4. Comparing the Two Estimates

[16] We now compare the updated estimates from BBHR, shown in Figures 3b and 3e, and those from HadGEM2-A,
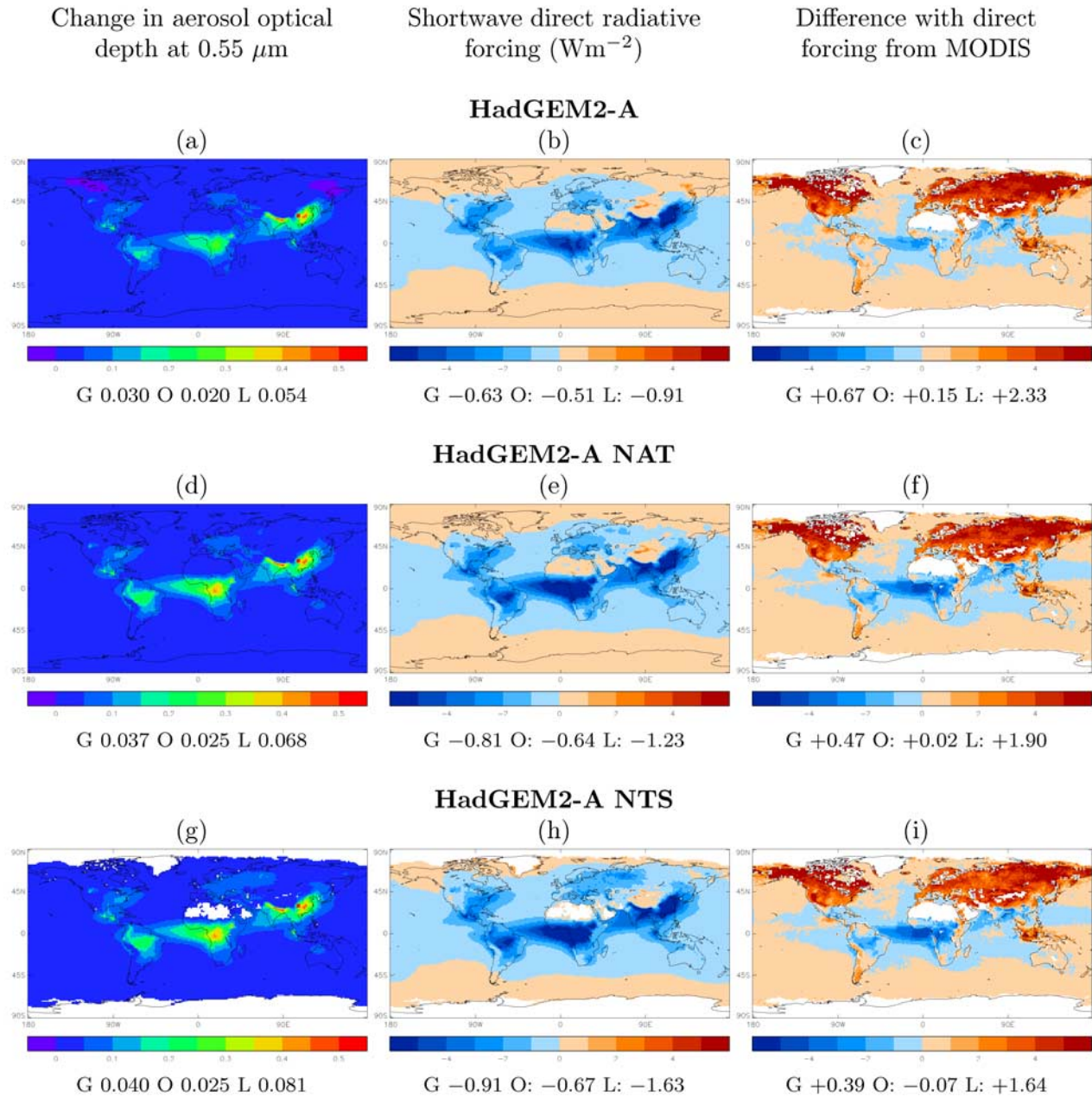
Figure 4. Annual distributions of the change in aerosol optical depth (left column) and clear-sky shortwave direct radiative forcing (middle) as simulated by the Hadley Centre climate model HadGEM2-A with respect to (a–c) 1860, (d–f) present-day natural aerosols, (g–i) present-day natural aerosols and sampled according to MODIS missing data mask on a monthly basis. Panels c, f, and i give the difference between the HadGEM2-A direct forcing and that derived from MODIS retrievals, as shown in Figure 3e. Averages are given on a global (G), ocean-only (O), and land-only (L) basis.

shown in Figures 4a and 4b. Ocean, land, and global averages are summarized in Table 2. BBHR and HadGEM2-A estimates differ significantly, with a factor of two difference in their global clear-sky DRFs. Figure 4c shows the difference between modeled and BBHR distributions. Positive values indicate where the BBHR estimate is more negative than that from HadGEM2-A: mainly northern hemisphere continents. The land-averaged difference is very large at +2.33 Wm^{-2}. Conversely, areas where the BBHR estimate is less negative than that from

HadGEM2-A are indicated by negative values, and mainly cover ocean areas.

[17] Putting aside for the moment differences in assumed aerosol optical properties, there are three different reasons why observation- and modeling-based estimates may be expected to differ. First, the two estimates calculate DRF based on a different change in aerosol optical depth. Second, the Earth's surface is not entirely covered by observations. Third, the cloudy-sky forcing has to be assumed by satellite-based studies when trying to provide

Table 2. Yearly Averaged Change in Aerosol Optical Depth or Anthropogenic Optical Depth (Both Noted $\Delta\tau$) at 0.55 μm and Resulting Direct Radiative Forcing (DRF, Wm^{-2}) and Normalized Direct Radiative Forcing (nDRF, Wm^{-2} per Unit Optical Depth) in the Shortwave Spectrum[a]

	Ocean			Land			Global		
	$\Delta\tau$	Clear-Sky DRF	Clear-Sky nDRF	$\Delta\tau$	Clear-Sky DRF	Clear-Sky nDRF	$\Delta\tau$	Clear-Sky DRF	All-Sky DRF
BBHR (Collection 5)	0.021	−0.60	−28.6	0.107	−3.27	−30.6	0.043	−1.30	−0.65
HadGEM2-A	0.020	−0.51	−25.5	0.054	−0.91	−16.9	0.030	−0.63	−0.16
HadGEM2-A NAT	0.025	−0.64	−25.6	0.068	−1.23	−18.1	0.037	−0.81	−0.25
HadGEM2-A NTS	0.025	−0.67	−26.8	0.081	−1.63	−20.1	0.040	−0.91	−0.28
HadGEM2-A CLD									−0.47

[a]BBHR is the method of *Bellouin et al.* [2005] applied to MODIS collection 5 data for 2002. HadGEM2-A is the Hadley Centre climate model. HadGEM2-A NAT uses present-day natural aerosols to approximate preindustrial distributions. HadGEM2-A NTS does the same and is also sampled according to the areas observed by BBHR. HadGEM2-A CLD assumes in addition that the cloudy-sky contribution to the all-sky DRF is zero.

an all-sky estimate. In the following, we import the assumptions (and shortcomings) of the BBHR method into the climate model in order to reconcile both estimates.

4.1. Natural Versus Preindustrial

[18] Following the IPCC definition, direct forcing is exerted by the increase in total AOD due to anthropogenic activities since preindustrial times (assumed to be 1750 by *Forster et al.* [2007] and 1860 in HadGEM2-A); in BBHR, it is the consequence of the presence of present-day anthropogenic aerosols. Therefore, the HadGEM2-A change in AOD is, by construction, smaller than the anthropogenic AOD in BBHR. This is primarily because of anthropogenic biomass-burning aerosols which were already present in 1860, albeit with smaller optical depths than they have now. To assess the impact of using natural aerosols as an approximation of preindustrial ones, the change in optical depth and the resulting forcing have also been computed in HadGEM2-A as the difference between a simulation including all present-day aerosols and a simulation that only includes those aerosols of natural origin: mineral dust, sea-salt, and ammonium sulphate from DMS emissions and volcanos. A certain amount of biomass-burning may well be of natural origin, but without the information required to determine how much, all biomass-burning aerosols are considered anthropogenic in the model: this assumption is also made in the BBHR algorithm. Results, identified as HadGEM2-A NAT, are shown in Table 2 and in Figures 4d to 4f. As expected, the change in AOD increases, especially in biomass-burning regions. The clear-sky DRF becomes more negative by one third on a global average. Over ocean, the model now simulates a clear-sky DRF that is more negative than the value obtained by the BBHR algorithm (−0.64 and −0.60 Wm^{-2}, respectively). This change is mainly driven by the modeled DRF being more negative over the Gulf of Guinea where transported biomass-burning aerosols are present. Differences in aerosol absorption are discussed in section 4.5. Over land, the very large discrepancies between the two distributions continue to exist, albeit with a land-averaged difference reduced from +2.33 to +1.90 Wm^{-2}. On a global average, the change in AOD in HadGEM2-A is 14% smaller than BBHR's anthropogenic AOD. The clear-sky DRF is 38% less negative in the model, and the all-sky DRF is 61% less negative. Although we have moved toward an agreement, there are still significant differences left unexplained.

4.2. Observational Coverage

[19] As previously stated, MODIS can only retrieve the total AOD in favorable conditions. Consequently, a given area is not associated with a valid retrieval everywhere and everyday. Figure 5 shows the fraction of 1° by 1° ocean or land grid boxes yielding a valid monthly average of anthropogenic AOD as estimated by BBHR for three regions. In the extratropical northern hemisphere, estimates of the anthropogenic AOD covers a much larger fraction of land and ocean grid boxes during the period April to September than during the rest of the year. This is due to lacking retrievals over snow- and ice-covered surfaces, as well as during nighttime. Since the photochemical reactions that produce anthropogenic aerosols over industrialized areas are more active during the summer, the high summertime anthropogenic AODs will be better sampled than the low wintertime ones. This results in the annual-averaged anthropogenic AOD being biased high in BBHR. In the tropics, the fraction of valid monthly averaged anthropogenic AODs is large and stable throughout the year. The seasonality of biomass-burning events is therefore likely to be well represented in the observation-based estimates. The 20% of land grid boxes that are consistently not observed correspond to desert areas, especially the Sahara. There, anthropogenic AODs are expected to be small but the surface brightness is enough to make the DRF switch sign and become positive. Such positive numbers are included in the global average from the model, but not in BBHR values. In the extratropical southern hemisphere, the fraction of ocean points covered reaches a minimum during the local winter, in June and July. The fraction of land covered is only around 10%, since AODs are not retrieved over ice-covered Antarctica. According to HadGEM2-A NAT simulations, those areas are associated with small anthropogenic AODs that will exert a DRF close to zero or again slightly positive.

[20] The modeled monthly distributions of the change in AOD and DRF, defined with respect to present-day natural aerosols, are now sampled according to the corresponding monthly coverage of MODIS. In doing so, although the number of points in the modeled averages is still different (MODIS retrievals are made on a daily basis), the area included in the monthly averages is the same. Estimates from the model now take the values given in Table 2 under the heading HADGEM2-A NTS. Corresponding distributions are shown in Figures 4g to 4i. Over ocean, the sampling removes high-latitude regions where the Sun is low or are consistently covered by clouds at the time of the
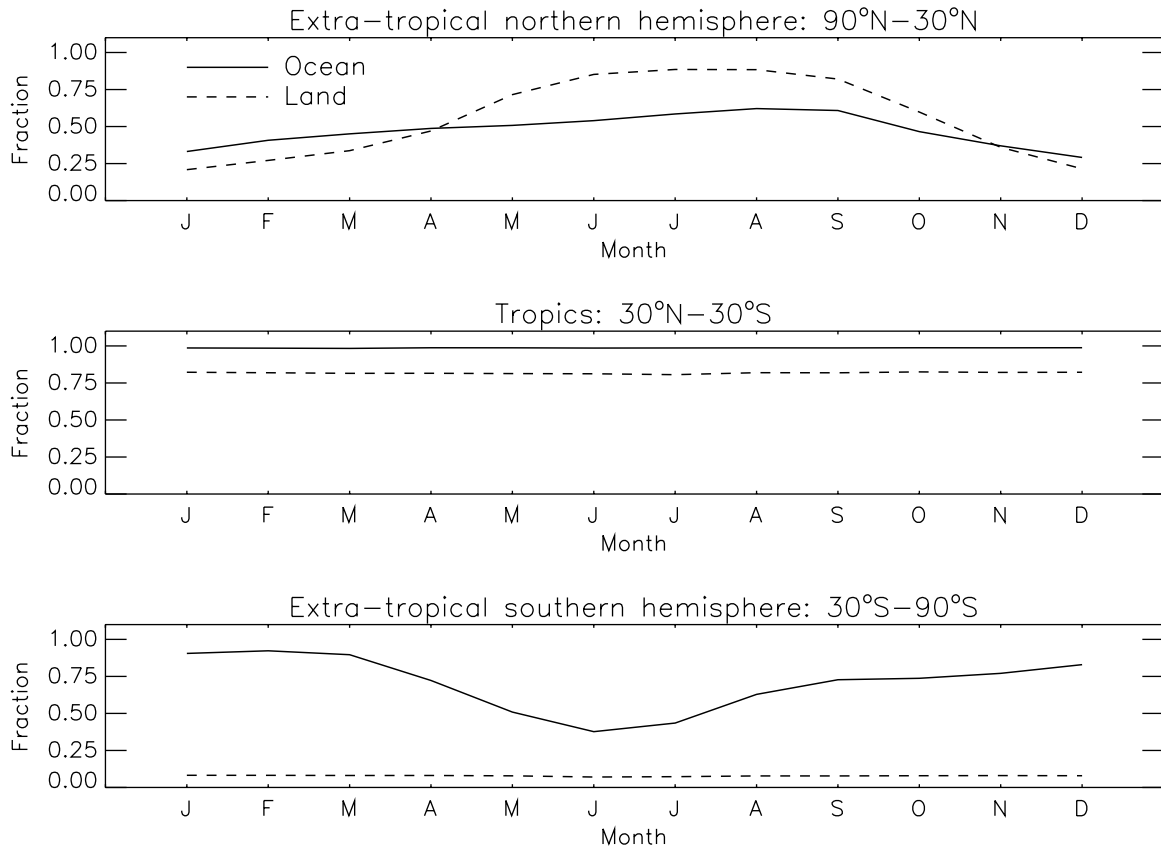
Figure 5. Fractions of ocean (solid lines) and land (dashed lines) grid-boxes having a valid monthly average of the anthropogenic aerosol optical depth in three regions. Anthropogenic aerosol optical depths are estimated using *Bellouin et al.* [2005] algorithm on MODIS collection 5 data for 2002.

satellite overpass. By removing the small anthropogenic AODs and slightly positive DRFs modeled there, the sampling does not alter the global-averaged anthropogenic AOD much but makes the clear-sky DRF slightly more negative. Over land, changes are more significant: the anthropogenic AOD at 0.55 μm increases from 0.068 to 0.081, and the clear-sky DRF becomes more negative and reaches -1.63 Wm^{-2}. Here again, the sampling has removed the small wintertime anthropogenic AODs from the annual average but at a much larger scale than over ocean. Globally averaged anthropogenic AOD and clear-sky DRF, which are mainly driven by their ocean contributions, become larger in magnitude. The distribution of the difference compared with BBHR still shows large values over northern hemisphere continents and averages $+1.64$ Wm^{-2} on land points. The change in AOD from HadGEM2-A is still 7% smaller than the anthropogenic AOD from BBRH, and the clear-sky DRF 30% less negative.

4.3. Uncertainties

[21] After defining the change in AOD and the DRF with respect to natural aerosols, and also sampling the modeled fields according to areas observed by MODIS, estimates of the DRF from the model and BBHR are still different. Over clear-sky oceans, there is a difference of 0.004 in the anthropogenic AOD and -0.07 Wm^{-2} in the DRF. Corresponding numbers are 0.026 and -1.64 Wm^{-2} over clear-sky land surfaces. If those differences are smaller than

the uncertainties in the estimates of both approaches, then it may be said that the two methods agree.

[22] BBHR used a Monte-Carlo method based on 250 runs of the algorithm to estimate the uncertainty (1 standard deviation) in anthropogenic AOD and clear-sky DRF. This uncertainty is a consequence of the uncertain parameters used in the algorithm, essentially the thresholds on the AMF for the anthropogenic AOD and aerosol absorption for the clear-sky DRF. The uncertainty in MODIS retrievals is considered a random error. In each run, algorithm parameters are randomly varied within their uncertainty range to assess the impact on the globally averaged anthropogenic AODs and DRF. Over ocean, the BBHR identification algorithm has an uncertainty of ±0.003 in the anthropogenic AOD and ±0.11 Wm^{-2} in the clear-sky DRF. Over land, the BBHR identification algorithm has larger uncertainties: ±0.021 in the anthropogenic AOD and ±0.85 Wm^{-2} in the clear-sky DRF. On a global average, uncertainties in the BBHR identification algorithm are ±0.01 for the anthropogenic AOD and ±0.3 Wm^{-2} for the clear-sky DRF.

[23] There are also uncertainties in the model. It is arguable that the model underestimates the anthropogenic AOD and DRF, since wintertime ammonium sulphate concentrations are underestimated compared with observations [*Bellouin et al.*, 2007], and other anthropogenic aerosol species, such as fossil-fuel organic carbon and nitrate aerosols, are not yet included. Note, however, that as far

(a) Clear-sky ocean
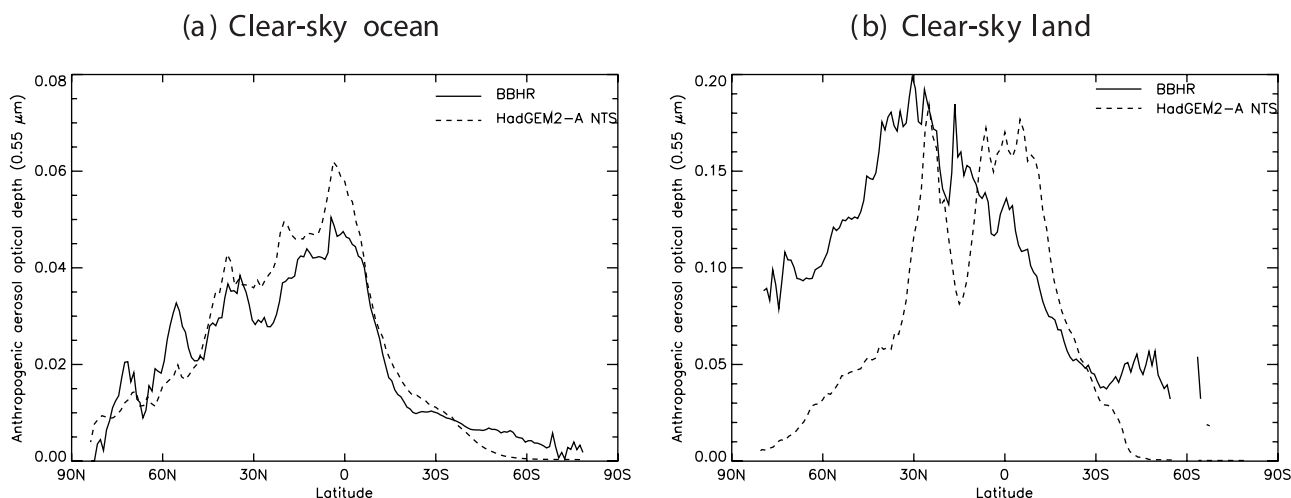
(b) Clear-sky land

Figure 6. Zonal distribution of the present-day anthropogenic aerosol optical depth at 0.55 μm as estimated from MODIS collection 5 retrievals (solid lines) and simulated by HadGEM2-A NTS (dashed lines) over clear-sky ocean (left) and land (right) surfaces.

as our comparison is concerned, any wintertime deficiencies in the modeled aerosols have a reduced impact over northern hemisphere continents due to sampling according to MODIS retrievals. The AeroCom project also showed that anthropogenic AODs and DRFs vary between models due to uncertainties in estimating aerosol emissions and modeling aerosol processes. For participating models, the variability amounted to ±0.3 Wm^{-2} in the clear-sky DRF on a global average. Another likely cause of disagreement between models and observations is the year-to-year variability of aerosol concentrations, which precludes a perfect match between a single year of observation and model simulations for "present-day" conditions.

[24] For the clear-sky DRF over ocean, differences between BBHR and HadGEM2-A are within the uncertainties. In contrast, despite the larger uncertainties in BBHR estimates over land, the differences with HadGEM2-A are not within the uncertainties of the BBHR algorithm.

4.4. Zonal Means

[25] Figure 6 shows the zonal distribution of the anthropogenic AOD in BBHR and HadGEM2-A NTS, over ocean and land surfaces. Note that the statistical significance of the annual mean varies with latitude, since the number of daily retrievals for the year 2002 is not homogeneous throughout the globe (Figure 2h). Over ocean, BBHR and the model locate the anthropogenic aerosols at similar latitudes. Indeed, the agreement in the zonal mean anthropogenic AOD is remarkable given that it is derived entirely from measurements in BBHR and entirely from the model in HadGEM2-A NTS. Over land, however, BBHR shows much larger anthropogenic AODs north of 30°N. These differences could be due to a combination of overestimated total AODs retrieved by MODIS, underestimated anthropogenic AODs simulated by the climate model, and/or wrong anthropogenic fractions applied to the MODIS retrieval. In the following, each of these three possibilities is reviewed in turn.

[26] Retrieving aerosol properties from space over land surfaces is made difficult by the surface contribution to the measured signal. For this reason, the AMF is not available

from MODIS over land, and the retrieved AOD may be less accurate than over ocean. In order to assess whether MODIS AODs are biased high, a comparison against AERONET measurements is made in three regions (Europe, North America, and Asia) located north of 30°N where the MODIS zonal mean is significantly larger than that from the climate model. AERONET measurements are daily-averaged AODs from the direct sun algorithm version 2, at the quality-assured level 2.0. The AOD at 0.55 μm is computed from that at 0.44 μm and the Angström exponent between 0.44 and 0.87 μm. The list of AERONET sites used in the comparison and the number of daily averages available for 2002 are given in Table 3. Daily averages made out of less than 10 measurements in that day are not considered. These averages are compared against the MODIS retrieval in the 1° × 1° gridbox where the AERONET site is located. An assessment of the MODIS aerosol retrieval algorithm would require a higher resolution and selecting the AERONET measurement taken within 30 minutes of Terra's overpass. However, it is assumed that using MODIS/Terra product MOD08_D3 fairly represents aerosols throughout the day and across the grid box, and this assumption, along with the performance of the MODIS algorithm, is tested in this comparison. The number of days when AERONET and MODIS both provide a daily value are given for each AERONET site in Table 3. This number is systematically smaller than the number of daily averages available from AERONET, since MODIS retrievals can be prevented by clouds or too high a surface reflectance at the time of Terra's overpass. As expected from the time evolution of the coverage of northern continents by MODIS (Figure 5), the June–August period sees the larger number of days when both AERONET and MODIS provide a valid total AOD (41% of the total) while the December–February period is associated with the smaller number (13%). Spring and autumn yield 21% and 25% of the comparison opportunities, respectively. Results of the comparison are shown in the left-hand side column of Figure 7 as point-density plots with AOD bins of 0.05. Plots exhibit a significant amount of scatter, which can be expected from the con-

Table 3. List of AERONET Sites Used to Compare Against MODIS Retrievals and HadGEM2-A Simulations[a]

Site Name	Coordinates	N_D	$N_{combined}$	N_{month}
Europe North of 30°N				
Andenes	69N−16E	13	13	2
Avignon	43N−4E	149	137	12
Belsk	51N−20E	77	68	9
Bordeaux	44N−0W	118	104	12
El Arenosillo	37N−6W	177	162	12
Fontainebleau	48N−2E	73	52	10
Gotland	57N−18E	121	110	9
Helgoland	54N−7E	10	7	5
IFT-Leipzig	51N−12E	68	49	12
IMC Oristano	39N−8E	190	131	12
ISDGM CNR	45N−12E	128	113	10
Ispra	45N−8E	176	144	12
Lille	50N−3E	27	19	6
Minsk	53N−27E	43	34	4
Modena	44N−10E	111	94	8
Moldova	47N−28E	143	120	12
Moscow MSU MO	55N−37E	120	100	11
Munich Maisach	48N−11E	59	50	8
Nes Ziona	31N−34E	91	61	11
Oostende	51N−2E	48	38	7
Palaiseau	48N−2E	26	21	6
Pitres	36N−3W	8	7	1
Rome Tor Vergata	41N−12E	84	73	7
The Hague	52N−4E	78	62	12
Toravere	58N−26E	64	57	4
Venise	45N−12E	175	147	12
North America North of 30°N				
Barrow	71N−156W	49	25	7
Bermuda	32N−64W	130	86	11
Bonanza Creek	64N−148W	93	68	8
Bondville	40N−88W	93	69	12
BSRN BAO Boulder	40N−105W	229	126	12
CARTEL	45N−71W	100	61	11
Cart Site	36N−97W	100	79	9
CCNY	40N−73W	147	132	12
Churchill	58N−93W	25	14	3
Columbia SC	34N−81W	156	130	10
Corcoran	36N−119W	176	172	8
COVE	36N−75W	194	166	12
Fresno	36N−119W	205	197	9
GISS	40N−73W	96	87	9
GSFC	38N−76W	202	172	12
Halifax	44N−63W	79	70	7
HJ Andrews	44N−122W	72	58	6
Howland	45N−68W	57	36	8
KONZA EDC	39N−96W	227	175	12
Maricopa	33N−111W	161	126	9
MD Science Center	39N−76W	182	157	12
Norfolk State U.	36N−76W	102	90	7
Railroad Valley	38N−115W	120	88	7
Rimrock	46N−116W	167	159	11
Rogers Dry Lake	34N−117W	302	275	12
San Nicolas	33N−119W	79	54	8
Saturn Island	48N−123W	123	105	9
SERC	38N−76W	114	106	9
Sevilleta	34N−106W	278	225	12
SMEX	41N−93W	22	20	2
Sioux Falls	43N−96W	98	75	9
Stennis	30N−89W	92	76	8
Thompson	55N−97W	55	49	6
UCLA	34N−118W	146	152	11
Asia North of 30°N				
Beijing	39N−116E	128	111	9
Dalanzadgad	43N−104E	191	84	12
Gosan SNU	33N−126E	13	8	5
Krasnoyarsk	55N−92E	56	44	6
Osaka	34N−135E	98	79	12
Seoul SNU	37N−126E	58	56	9

Table 3. (continued)

Site Name	Coordinates	N_D	$N_{combined}$	N_{month}
Shirahama	33N−135E	93	82	10
Tomsk	56N−85E	5	5	2

[a]N_D is the number of daily averages made out of more than 10 measurements in 2002. $N_{combined}$ is the number of AERONET averages with a corresponding retrieval in the MOD08_D3 product for the same year. N_{month} is the number of monthly averages made out of at least 10 days in 2002.

ditions of the comparison. In Europe and North America, the performance of MODIS is satisfactory, while the total AOD might be underestimated in Asia, although the smaller number of AERONET sites decreases the value of the fit. There appears to be no evidence for a significant and systematic high bias in the total AOD given in MOD08_D3 products.

[27] The performance of HadGEM2-A at simulating total aerosol optical depths is assessed using a similar comparison against AERONET, presented in the right-hand side column of Figure 7. This comparison is done slightly differently than that used to assess the performance of MODIS. First, since the climate model simulates its own meteorology, it is not expected to match AERONET on a daily basis. Monthly averages from both AERONET and the model are therefore compared. For AERONET, monthly averages must be made out of at least 10 days to be retained. The number of monthly averages available in 2002 for each AERONET site is given in Table 3. The second difference is that AODs are given at 0.44 μm. Results show that the model does not reproduce AERONET measurements as well as MODIS does. The model underestimates the total AOD in Europe and, to a smaller extent, in North America and Asia. This underestimation may stem from incorrect emission data sets of aerosols or their precursors, incorrect simulation of the life cycle and transport of aerosols, and/or missing aerosol species. Since anthropogenic nitrates are one of those missing aerosol species, the anthropogenic AOD simulated by the model is likely to be too small. However, the successful comparison achieved against BBHR for anthropogenic AODs transported over ocean suggests that the underestimation of the total AOD over land may well be primarily due to missing natural aerosols.

[28] At this point, MODIS total AODs used by the BBHR algorithm have been shown to satisfactorily compare against AERONET, while HadGEM2-A's performance is not as good. However, Figure 6 does not present total AODs but anthropogenic AODs. From the original MODIS retrieval, there is one more step involved over land: multiplying by the model-derived regional anthropogenic fractions. The two regions covering the northern hemisphere north of 30°N are associated with large and uncertain anthropogenic fractions: 0.56 ± 0.21 for North America and 0.54 ± 0.16 for Eurasia [BBHR]. The zonal means of the annual-averaged total AODs as simulated by the five AeroCom models used to provide the anthropogenic fractions (see section 2.1) are shown in Figure 8. Also shown in Figure 8 are the corresponding zonal mean from MODIS and HadGEM2-A NTS. All models have been sampled according to the MODIS availability mask. There are different behaviours among models and, in general, they fail at reproducing the MODIS-retrieved total AODs north of
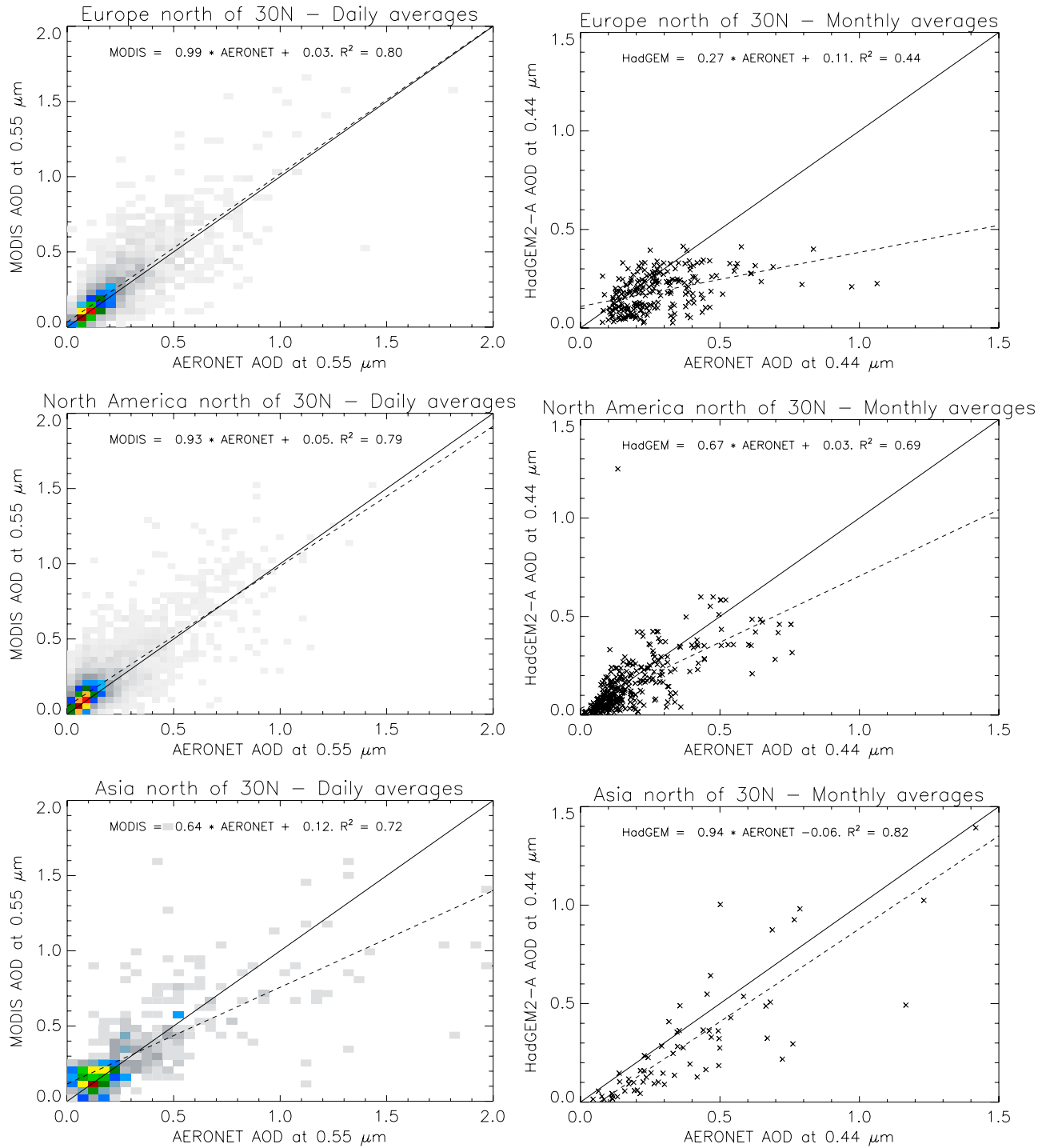
Figure 7. Left: daily-averaged total aerosol optical depth at 0.55 μm from MODIS MOD08_D3 collection 5 against that from AERONET version 2 level 2.0 for 2002. Coloured boxes indicate the percentage of total points in aerosol optical depth bins of 0.05 by 0.05. Right: monthly total aerosol optical depth at 0.44 μm from HadGEM2-A against that from AERONET. AERONET sites are listed in Table 3. Values from MODIS and HadGEM2-A are those for the gridbox that contains the AERONET site. The 1-to-1 line is the solid line, and the best linear fit is indicated by the dashed line.

30°N. HadGEM2-A does not fare well and simulates lower total AODs. One could argue that, as far as the anthropogenic fraction is concerned, the value of the total AOD is of secondary importance, since it measures the respective weight of anthropogenic and natural aerosols. However, should the AOD missing from models over land be mainly of natural origin, the anthropogenic fraction would be over-estimated, leading to overestimated anthropogenic AODs
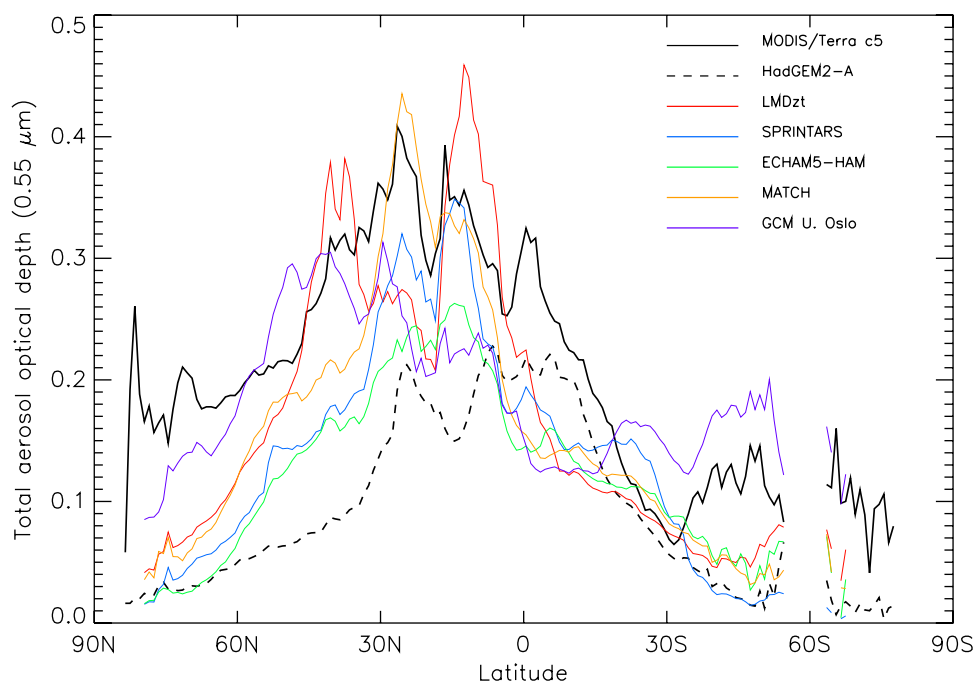
Figure 8. Zonal mean of the annual-averaged total aerosol optical depth for MODIS (black line) collection 5 for 2002, and selected AeroCom models simulating present-day conditions (coloured lines). The Hadley Centre climate model HadGEM2-A is shown by the black dashed line.

and DRF from the BBHR algorithm. Validating the anthropogenic fraction over land in both polluted and more remote areas, or replacing it by an observed quantity (e.g., the AMF when it is retrieved reliably from space over land) are steps needed for improving the quality of the BBHR estimate of DRF over land.

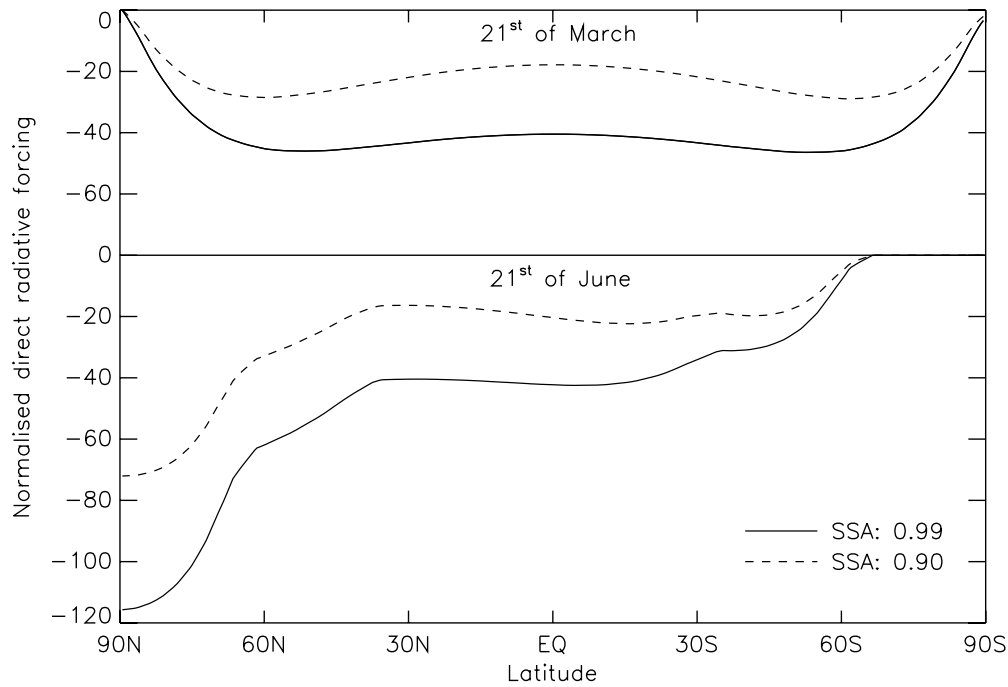### 4.5. Normalized Direct Radiative Forcing

[29] The normalized direct radiative forcing (nDRF), also referred to as the radiative forcing efficiency, is the DRF per unit aerosol optical depth. For BBHR and HadGEM2-A NTS, the DRF is defined with respect to present-day natural aerosols and the AOD is that of present-day anthropogenic aerosols. As shown in Table 2, BBHR and HadGEM2-A NTS have similar values of the nDRF over ocean. Over land, however, they differ significantly, with aerosols in BBHR being more efficient at exerting DRF per unit AOD.

[30] Since daily-integrated DRFs depend on the distribution of the solar zenith angle, the nDRF depends on the day of the year and the latitude, as well as on the aerosol absorption and vertical profile, and the surface albedo. For illustration purposes, Figure 9 shows the zonal distribution of the nDRF for an accumulation-mode aerosol with a monomodal lognormal distribution of the number characterized by a modal radius of 0.095 μm and a standard deviation of 0.34, with an AOD of 0.15 at 0.55 μm. Two different aerosol absorptions are presented. The first, corresponding to a sulphate aerosol, is obtained by using a wavelength-independent complex refractive index of $1.53 - 10^{-7}i$ and yields a single-scattering albedo of 0.99 at 0.55 μm. The second, corresponding to a biomass-burning aerosol, uses a refractive index of $1.54 - 0.018i$ and yields a single-scattering albedo of 0.90. The shortwave surface albedo is 0.1. Zonal distributions are computed for the spring

equinox and the northern hemisphere summer solstice. At midlatitudes, solar zenith angles remain at intermediate values where the instantaneous direct radiative effect is stronger [*Boucher et al.*, 1998]. Therefore, midlatitude aerosols have a stronger nDRF than aerosols located near the equator. This is not a negligible effect: the nonabsorbing aerosol has a nDRF which is 20 Wm^{-2} per unit AOD more negative at 60°N than when it is located between 30°N and the equator in summer. The effect of increasing aerosol absorption is to decrease the nDRF since, contrary to scattering, absorption does not increase the outgoing flux at the top of the atmosphere.

[31] In the previous section, anthropogenic AODs have been shown to be much better colocated between BBHR and HadGEM2-A NTS over ocean than over land. Over land, anthropogenic AODs from BBHR are much larger north of 30°N. As those anthropogenic AODs were mainly retrieved during spring and summer (Figure 5), they translate into a stronger nDRF, as illustrated by Figure 9. In contrast, HadGEM2-A NTS aerosols are located closer to the equator and are associated with weaker nDRFs. To quantify this effect, the DRF that would be exerted by the anthropogenic aerosols apparently missing from the model over land is approximated by multiplying the difference in anthropogenic AOD between BBHR and HadGEM2-A NTS by the nDRFs shown in Figure 9. North of 30°N, the non-absorbing aerosol is used. The more absorbing aerosol is used at the other latitudes. Doing so yields a missing DRF of −1.48 and −1.98 Wm^{-2} for spring and summer distributions, respectively. Since the difference in annual-averaged DRF between BBHR and HadGEM2-A NTS is −1.64 Wm^{-2}, this simple calculation shows that the differing locations of anthropogenic aerosols over land can explain differences in nDRF.

Figure 9. Zonal distribution of the normalised direct radiative forcing (Wm^{-2} per unit aerosol optical depth) computed for an accumulation-mode aerosol (see text) at an aerosol optical depth of 0.15 and a single-scattering albedo of 0.99 (solid lines) and 0.90 (dashed lines) at 0.55 μm. The top section of the plot is for the spring equinox and the bottom section is for the summer solstice, where seasons are for the northern hemisphere. Shortwave surface albedo is 0.1.

[32] Additionally, as shown in Figure 9, aerosol absorption also plays a role in determining the nDRF. Table 4 shows the single-scattering albedo at 0.55 μm of anthropogenic aerosols for six regions, as prescribed in BBHR and simulated in HadGEM2-A. Northern hemisphere industrial aerosols are typically more absorbing in the model than in BBHR, while the opposite is true in regions where biomass-burning aerosols are expected to be the main contributor to the anthropogenic AODs. Therefore, in addition to locating its aerosols where they have a stronger nDRF, in those locations BBHR uses a more scattering aerosol, which will exert an even stronger nDRF at the top of the atmosphere. Near the equator, the nDRF in BBHR will be smaller than that in HadGEM2-A, but this is dominated by what is happening further north. In addition to differing aerosol locations and absorbing properties, other assumptions made in BBHR and the climate model will induce different normalized DRFs. In BBHR, important assumptions are the aerosol vertical profile, the optical properties of the unidentified natural aerosol over land, and regional size distributions. Where any one of these assumptions is wrong, sensitivity tests indicate that the estimated DRF may be underestimated or overestimated.

4.6. Cloudy-Sky and All-Sky Forcing

[33] Even after sampling the model in a similar manner to the satellite retrievals, the all-sky DRF in HadGEM2-A of -0.25 Wm^{-2} remains 57% less negative than the BBRH value of -0.65 Wm^{-2}. This is almost twice the difference in clear-sky forcing and means that an additional cause for disagreement has been introduced in the all-sky estimates.

The all-sky DRF, ΔF_{all}, can be written in terms of its cloudy (ΔF_{cloud}) and clear (ΔF_{clear}) contributions as

$$\Delta F_{all} = C \; \Delta F_{cloud} + (1 - C) \; \Delta F_{clear} \qquad (6)$$

where C is the fractional cloud cover. In order to account for the spatial correlation between cloud cover and aerosol concentrations, equation (6) should be computed at each time step before any temporal averaging [*Haywood and Shine*, 1997]. However, in order to match calculations made by *Schulz et al.* [2006], annual-averaged distributions are used in equation (6). Modeled distributions of the cloudy- and all-sky DRFs are shown in Figure 10. Positive forcings happen where absorbing biomass-burning aerosols off the shores of Namibia and industrial carbonaceous aerosols in East Asia overlie low clouds. In HadGEM2-A, the globally averaged cloudy-sky DRF is +0.3 Wm^{-2} when computed with respect to 1860 conditions. For AeroCom models,

Table 4. Annual-Averaged Single-Scattering Albedo at 0.55 μm for Anthropogenic Aerosols in the Work of *Bellouin et al.*, [2005] (BBHR) and the Hadley Centre Climate Model, HadGEM2-A[a]

Region	Boundaries	BBHR	HadGEM2-A
North America	90°N–30°N 180°W–30°W	0.98 ± 0.02	0.91
Eurasia	90°N–30°N 30°W–180°E	0.94 ± 0.03	0.91
Central America	30°N–0° 120°W–60°W	0.91 ± 0.03	0.94
South America	30°N–90°S 180°W–30°W	0.86 ± 0.015	0.93
Africa, Oceania	30°N–90°S 30°W–180°E	0.90 ± 0.02	0.95
Indian Ocean	30°N–10°S 30°E–120°E	0.91 ± 0.03	0.93

[a]Regions are those used in the work of *Bellouin et al.* [2005] to prescribe absorbing properties.

Shortwave direct radiative forcing
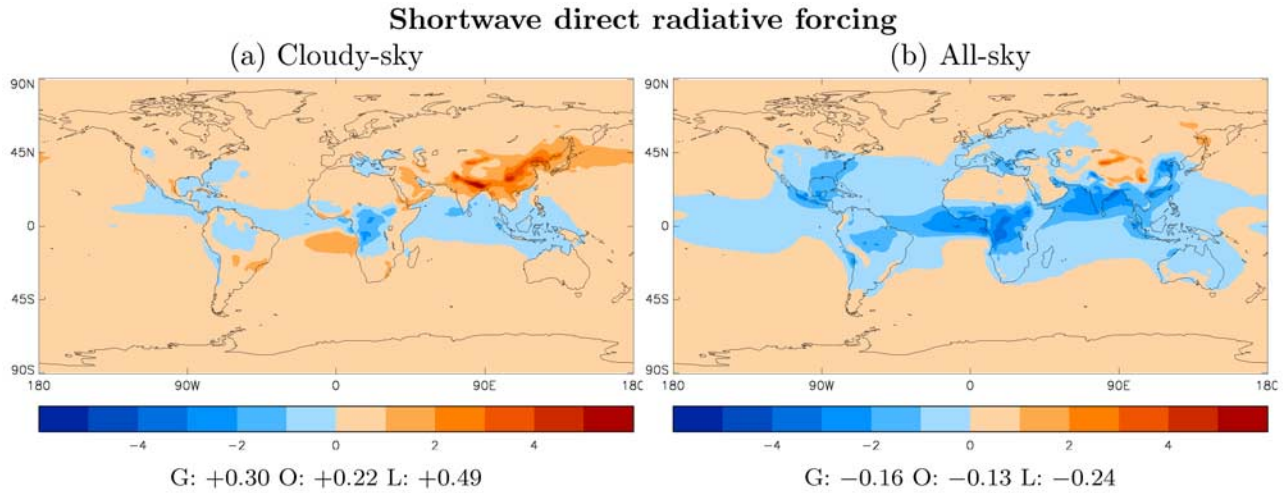
Figure 10. Shortwave direct radiative forcing (Wm^{-2}) as simulated by the Hadley Centre climate model HadGEM2-A in (a) cloudy-sky and (b) all-sky (clear plus cloudy) conditions with respect to 1860. Averages are given on a global (G), ocean-only (O), and land-only (L) basis.

this forcing has very diverse values, ranging from −0.2 to +0.3 Wm^{-2} [*Schulz et al.*, 2006].

[34] Lacking cloudy-sky aerosol retrievals, BBRH assumed $\Delta F_{cloud} = 0$ and, compared with HadGEM2-A, this assumption leads to an all-sky forcing which is too negative. Using equation (6), the all-sky forcing from HadGEM2-A NTS is recomputed using the BBRH assumption that the cloudy-sky forcing is zero. In doing so, the modeled all-sky forcing nearly doubles in absolute value, from −0.28 to −0.47 Wm^{-2} (Table 2 under HadGEM2-A CLD). The latter value is 28% less negative than the BBRH estimate, a difference now similar to that between HadGEM2-A and BBRH estimates of the clear-sky forcing on a global average.

5. Conclusion

[35] *Bellouin et al.* [2005] published an algorithm to identify the anthropogenic fraction of the total aerosol optical depth observed by MODIS. When applied to MODIS collection 4 retrievals it yields a clear-sky aerosol direct radiative forcing of −1.89 Wm^{-2} on a global average for 2002. Here, the same algorithm has been applied to MODIS collection 5 retrievals and yields the less negative value of −1.30 Wm^{-2}. This latter estimate is still more negative than the −0.63 Wm^{-2} simulated by the Hadley Centre climate model HadGEM2-A.

[36] Three causes for the disagreement between observation- and modeling-based estimates of the anthropogenic aerosol optical depth and direct radiative forcing have been identified. First, the assumption that present-day natural aerosols are a good proxy for preindustrial aerosols leads to larger inferred changes in aerosol optical depth in the observation-based estimate. Second, annual and global averages from satellite-based studies are biased towards ocean and summertime continental areas, due to the inability to retrieve aerosol parameters everywhere on the Earth's surface. Third, the assumption that the cloudy-sky direct forcing is zero, used to scale the observation-based clear-sky estimates to all-sky, is not consistent with some climate

model simulations. The impact of these three items has been quantified by incorporating the assumptions made by the observation-based study of *Bellouin et al.* [2005] into simulations from the Hadley Centre climate model HadGEM2-A. Since *Bellouin et al.* [2005] and HadGEM2-A are typical examples of observation-based and modeling studies respectively, many of the results presented in this study will hold true for other observation-based methods and numerical models.

[37] Over clear-sky oceans, the anthropogenic aerosol optical depths derived from MODIS collection 5 data appears to be in a remarkable agreement with those from the HadGEM2-A model, and the direct radiative forcing is also in agreement. Assuming that preindustrial aerosol optical depths are correctly simulated over ocean by the model, there is no reason to think that the model underestimates the aerosol radiative forcing with respect to preindustrial conditions. Over clear-sky land surfaces, the situation is very different. The quality of the anthropogenic aerosol optical depths derived by the *Bellouin et al.* [2005] algorithm over land is unquantified and the confidence in the direct forcing is therefore low. Consequently, the model performance can currently not be evaluated over land surfaces. The same is true in cloudy skies and hence for all-sky averages. The large variability among models reported by *Schulz et al.* [2006] stresses the fact that it is also an open question in numerical modeling.

[38] In order to provide a useful constraint, observation-based estimates of the direct radiative forcing should be entirely independent of numerical models. Currently, even the least model-dependent algorithm of those listed in Table 1, by *Bellouin et al.* [2005] has to rely on models to provide an anthropogenic fraction of aerosol optical depth over land areas. To further improve satellite- and modeling-based estimates, improved satellite retrievals over land are obviously required together with a comprehensive validation strategy. Alternatively, it is likely that climate models will assimilate satellite observations of aerosols, reducing the need for independent, observation-based estimates of aerosol radiative forcings.

References

Bellouin, N., O. Boucher, J. Haywood, and M. S. Reddy (2005), Global estimate of aerosol direct radiative forcing from satellite measurements, *Nature*, *438*, 1138–1141.

Bellouin, N., et al. (2007), Improved representation of aerosols for Had-GEM2, Hadley Cent. Tech. Note 73, 43 pp., Met Office, Exeter, UK. (Available at http://www.metoffice.gov.uk/research/hadleycentre/pubs/HCTN/index.html.)

Boucher, O., et al. (1998), Intercomparison of models representing direct shortwave radiative forcing by sulfate aerosols, *J. Geophys. Res.*, *103*(D14), 16,979–16,998.

Christopher, S. A., J. Zhang, Y. J. Kaufman, and L. A. Remer (2006), Satellite-based assessment of top of atmosphere anthropogenic aerosol radiative forcing over cloud-free oceans, *Geophys. Res. Lett.*, *33*, L15816, doi:10.1029/2005GL025535.

Chung, C. E., V. Ramanathan, D. Kim, and I. Podgorny (2005), Global anthropogenic aerosol direct forcing derived from satellite and ground-based observations, *J. Geophys. Res.*, *110*, D24207, doi:10.1029/2005JD006356.

Collins, W. D., et al. (2002), Simulation of aerosol distributions and radiative forcing for INDOEX: Regional climate impacts, *J. Geophys. Res.*, *107*(D19), 8028, doi:10.1029/2000JD000032.

Cox, C., and W. Munk (1954), Statistics of the sea surface derived from sun glitter, *J. Mar. Res.*, *13*, 198–227.

Dentener, F., et al. (2006), Emissions of primary aerosol and precursor gases in the years 2000 and 1750, prescribed data-sets for AeroCom, *Atmos. Chem. Phys.*, *6*, 4321–4344.

Dubovik, O., et al. (2002), Variability of absorption and optical properties of key aerosol types observed in worldwide locations, *J. Atmos. Sci.*, *59*, 590–608.

Forster, P., et al. (2007), Changes in atmospheric constituents and in radiative forcing, in *Climate Change 2007: The Physical Science Basis. Contribution of Working Group I to the Fourth Assessment Report of the Intergovernmental Panel on Climate Change*, edited by S. Solomon et al., Cambridge Univ. Press, New York.

Haywood, J. M., and K. P. Shine (1997), Multi-spectral calculations of the direct radiative forcing of tropospheric sulphate and soot aerosols using a column model, *Q. J. R. Meteorol. Soc.*, *123*, 1907–1930.

Herman, J. R., et al. (1997), Global distribution of UV-absorbing aerosols from Nimbus7/TOMS data, *J. Geophys. Res.*, *102*, 16,911–16,922.

Kaufman, Y. J., D. Tanré, and O. Boucher (2002), A satellite view of aerosols in the climate system, *Nature*, *419*, 215–223.

Kaufman, Y. J., et al. (2005), Aerosol anthropogenic component estimated from satellite data, *Geophys. Res. Lett.*, *32*, L17804, doi:10.1029/2005GL023125.

Kirkevag, A., and T. Iversen (2002), Global direct radiative forcing by process parameterized aerosol optical properties, *J. Geophys. Res.*, *107*(D20), 4433, doi:10.1029/2001JD000886.

Levy, R. C., L. A. Remer, S. Mattoo, E. F. Vermote, and Y. J. Kaufman (2007), Second-generation operational algorithm: Retrieval of aerosol properties over land from inversion of Moderate Resolution Imaging Spectroradiometer spectral reflectance, *J. Geophys. Res.*, *112*, D13211, doi:10.1029/2006JD007811.

Martin, G. M., M. A. Ringer, V. D. Pope, A. Jones, C. Dearden, and T. J. Hinton (2006), The physical properties of the atmosphere in the new Hadley Centre Global Environmental Model, HadGEM1. Part 1: Model description and global climatology, *J. Clim.*, *19*, 1274–1301.

Reddy, M. S., et al. (2005), Estimates of global multi-component aerosol optical depth and direct radiative perturbation in the LMDZT General Circulation Model, *J. Geophys. Res.*, *110*, D10S16, doi:10.1029/2004JD004757.

Remer, L. A., et al. (2005), The MODIS aerosol algorithm, products, and validation, *J. Atmos. Sci.*, *62*, 947–973.

Schaaf, C. B., et al. (2002), First operational BRDF, albedo nadir reflectance products from MODIS, *Remote Sens. Environ.*, *83*, 135–148.

Schulz, M., et al. (2006), Radiative forcing by aerosols as derived from the AeroCom present-day and pre-industrial simulations, *Atmos. Chem. Phys.*, *6*, 5225–5246.

Smirnov, A., B. N. Holben, T. F. Eck, O. Dubovik, and I. Slutsker (2003), Effect of wind speed on columnar aerosol optical properties at Midway Island, *J. Geophys. Res.*, *108*(D24), 4802, doi:10.1029/2003JD003879.

Stier, P., et al. (2005), The aerosol-climate model ECHAM5-HAM, *Atmos. Chem. Phys.*, *5*, 1125–1156.

Takemura, T., T. Nozawa, S. Emori, T. Y. Nakajima, and T. Nakajima (2005), Simulation of climate response to aerosol direct and indirect effects with aerosol transport-radiation model, *J. Geophys. Res.*, *110*, D02202, doi:10.1029/2004JD005029.

Wentz, F. (1997), A well calibrated ocean algorithm for SSM/I, *J. Geophys. Res.*, *102*, 8703–8718.

Yu, H., et al. (2004), Direct radiative effect of aerosols as determined from a combination of MODIS retrievals and GOCART simulations, *J. Geophys. Res.*, *109*, D03206, doi:10.1029/2003JD003914.

N. Bellouin, A. Jones, and J. M. Haywood, Met Office Hadley Centre, FitzRoy Road, Exeter, Devon, EX1 3PB, UK. (nicolas.bellouin@metoffice.gov.uk)

S. A. Christopher, Department of Atmospheric Sciences, University of Alabama, 320 Sparkman Drive, Huntsville, AL 35805-1912, USA.